Industrial Crops & Products 222 (2024) 119825

Contents lists available at ScienceDirect

Industrial Crops & Products

journal homepage: www.elsevier.com/locate/indcrop

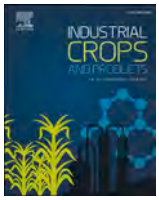

Green synthesis of silver nanoparticles from *Thymus vulgaris* and *Sambucus nigra* extracts in poly (vinyl alcohol) nanofiber matrix: *In vitro* evaluation

Ozlem Tavukcuoglu [a], Nilüfer Evcimen Duygulu [b,*], Aylin Altinbay [b], Fatih Ciftci [c,d,**]

[a] Faculty of Hamidiye Pharmacy, Department of Biochemistry, University of Health Sciences, Istanbul, Turkey
[b] Faculty of Chemical and Metallurgical Engineering, Department of Metallurgical and Material Engineering, Yildiz Technical University, Istanbul, Turkey
[c] Faculty of Engineering, Department of Biomedical Engineering, Fatih Sultan Mehmet Vakıf University, Istanbul, Turkey
[d] Department of Technology Transfer Office, Fatih Sultan Mehmet Vakıf University, Istanbul, Turkey

ARTICLE INFO

Keywords:
Black elderberry
Green synthesis
Nanocomposite
Thyme
Silver nanoparticles

ABSTRACT

In the current study, silver nanoparticles (AgNPs) green synthesized from *Thymus vulgaris* (Thyme) and *Sambucus nigra* (black elderberry) (BE) extracts and added into poly (vinyl alcohol) (PVA) solution to achieve antibacterial, biocompatible, and bioactive nanofibers through electrospinning technique. The absorbance peaks of AgNPs were found at 450 nm in the ultraviolet–visible (UV-Vis) spectrum, and AgNPs were found in (111) d-spacing in high-resolution transmission electron microscope (HRTEM). The average particle sizes were measured as 66.30 ± 7.70 nm and 20.03 ± 4.80 nm for ThymeAgNPs and BEAgNPs, respectively. 1 and 2 wt% content of the AgNPs were added into the PVA solution and electrospun at 9 kV voltage and 5 ml/hr flow rate. The fiber morphologies were investigated with the help of scanning electron microscopy (SEM) and HRTEM, and a decrease in the fiber diameter and the porosity of the fibers was obviously observed. Chemical bond analysis was done using Fourier transform infrared (FTIR), and the thermal behavior of the fiber was examined with a differential scanning calorimeter (DSC). X-ray diffraction (XRD) and HRTEM provide the presence of AgNPs in PVA nanofibers. According to antibacterial activity investigations the inhibition growth effect against *Escherichia coli* (*E. coli*) of PVA/ThymeAgNPs was 11.6 % higher than that of PVA/BEAgNPs. The cell cytotoxicity tests at different concentrations with L929 cells revealed better performance in PVA/Thyme nanofibers.

1. Introduction

Nanoparticles (NPs) are rising in material science, chemistry, molecular biology, physics, and medicine (Jamkhande et al., 2019). Nanoparticle synthesis can be achieved through chemical, physical, or biosynthesis, each with unique properties. Nanoparticle synthesis can be carried out by chemical, physical or biosynthesis, each with unique properties. However, the synthesis of nanoparticles by physical and chemical means has undesirable disadvantages such as toxicity problems, environmental pollution, and expensiveness. As a sustainable alternative, green synthesis has emerged as a key area of research due to its environmentally friendly nature and cost-effectiveness (Pal et al., 2018; Parveen et al., 2016). Green synthesis is carried out by using biological pathways such as bacteria, fungi or plants for the synthesis of nanoparticles with the help of various biotechnological techniques. Since the tendency to use natural products has increased, green synthesis of nanoparticles by plants has come to the forefront because it provides a fast, environmentally friendly, non-pathogenic and single-step technique. It is also a green chemistry approach that connects nanotechnology and plant biotechnology. The synthesis of metal nanoparticles using plant extracts occurs as a result of the reduction of metal ions by the phytochemical components of the plant (Hosseinzadeh et al., 2023; Lite et al., 2023; Roy et al., 2019). Phytochemical components such as phenolic compounds, flavonoids, and saponins found in plants act as metal ion reducing agents in the green synthesis of metal nanoparticles (Rajeshkumar and Bharath, 2017; Zhou et al., 2024). However, phytochemicals found in plant extracts vary depending on the type of plant. Therefore, the phytochemical components responsible for reduction in the green synthesis of metal nanoparticles using plant extracts are different (Alayande et al., 2021; Rajeshkumar and Bharath, 2017). Compared to previous approaches, this method allows for the synthesizing of nanoparticles (NPs) at smaller sizes, offering excellent

* Corresponding author.
** Corresponding author at: Faculty of Engineering, Department of Biomedical Engineering, Fatih Sultan Mehmet Vakıf University, Istanbul, Turkey.
E-mail addresses: nevci@yildiz.edu.tr, niluferduygulu@gmail.com (N. Evcimen Duygulu), fciftci@fsm.edu.tr, faciftcii@gmail.com (F. Ciftci).

https://doi.org/10.1016/j.indcrop.2024.119825
Received 31 August 2024; Received in revised form 3 October 2024; Accepted 8 October 2024

advantages regarding the NPs' ability to interact with cells (Parveen et al., 2016). The structure of the synthesized green nanoparticles demonstrates unique properties, such as aggregating or absorbing each other, as well as organic and inorganic molecules (Ong et al., 2014). Metal NPs have broken new ground in the field of NPs in the last few years (Bhattacharya and Mukherjee, 2008; Jamkhande et al., 2019). Among them, silver nanoparticles (AgNPs) are preferable because they have excellent physical-chemical properties and a wide range of uses (Prabhu and Poulose, 2012). AgNPs have special biological, optical, magnetic, electrical, and catalytic thermal properties, making them useful in various applications, including chemical, photovoltaic, and biological sensors. In addition, their high electrical conductivity and stability are other noteworthy features (Kulkarni and Muddapur, 2014). However, it's crucial to note that the most common application of AgNPs is their antimicrobial activities. Yet, it's essential to be aware that high concentrations of silver nanoparticles can lead to toxicity, underscoring the need for careful consideration and further research (Prabhu and Poulose, 2012). Today, incorporating NP into polymeric materials to increase their impact area is one of the preferred approaches. Electrospinning, a renowned technique, facilitates the integration of these NPs characteristics within the fibers. The continuity and stability of these fibers make them ideal nanoparticle carriers for diverse applications (Bao et al., 2010; Lu et al., 2016; Taghavi and Larson, 2014; Wang et al., 2011; Yanilmaz et al., 2016). The potential of nanoparticles in fibers is promising, hinging on factors such as homogeneous nanoparticle dispersion, interfacial interaction between polymer and nanoparticles, and particle size, shape, and phase (Ingram Taylor, 1969). Among the many polymers, PVA stands out for its unique semi-crystalline characteristics. Its non-toxic, biocompatible, and non-carcinogenic qualities add even more value. PVA's high hydrophilicity is a big help for electrospinning and composite films (El-Desoky et al., 2020). Another noteworthy characteristic is its excellent dimensional stability when exposed to UV–visible light, attributed to its unique molecular structure (Sinha et al., 2014). When AgNPs are introduced into PVA matrices, the resulting PVA/Ag nanofibers offer significant potential for diverse applications, including medical devices, wound dressings, and antimicrobial coatings (Dutta et al., 2020; Kaur et al., 2021; Nguyen and Le, 2021; Sau and Kundu, 2022).

Commonly known as thyme, *Thymus vulgaris* possesses potent antibacterial, antifungal, antiviral, antiseptic, and antioxidant qualities (Mousavian et al., 2021). The plant has been utilized for various medical conditions since ancient times (Manukumar et al., 2020). The thymol molecule found in its extract and essential oil can destabilize the bacterial membrane, killing bacteria (Ananda et al., 2017; Li et al., 2012; Nasrollahzadeh et al., 2016; Wang et al., 2015). Çimen et al. (Güneş Çimen et al., 2022) produced PCL/PLA nanofibers doped with AgNPs and encapsulated in *Thymus vulgaris* extract using electrospinning. They revealed its potential for cancer therapy in skin tumor cell lines. Melo et al. (De Melo et al., 2020) suggest using AgNPs biosynthesized using thyme essential oil as an antibacterial agent due to its high antibacterial activity against *Escherichia coli* and *Staphylococcus aureus*. Manukumat et al. (Manukumar et al., 2020) showed a membrane damage effect on their synthesized green thyme loaded silver nanoparticles against *Staphylococcus aureus*, besides maintaining remarkable blood compatibility. As well as medical applications, thyme could be used in long-lasting foodstuffs and be an option to prevent the development and spread of spoilage microorganisms (Boskovic et al., 2015; Nowak et al., 2012).

Conversely, elderberry, an alternative plant, has, antibacterial, anti-inflammatory, and anticancer characteristics (Krawitz et al., 2011; Sidor and Gramza-Michałowska, 2015; Wei et al., 2022). Jayakumar et al. developed poly(vinyl alcohol)/starch, titanium dioxide nanoparticles, and elderberry extract-based bio nanocomposites films with enhanced functional, mechanical, and water barrier properties and excellent antimicrobial activity to be used as active and intelligent food packing materials. They demonstrated that adding elderberry extract transformed the nanocomposite film into a possible pH sensor (Jayakumar et al., 2022). Black elderberry (*Sambucus nigra*, Adoxaceae), a cyanidin-rich berries, has been considered a suitable additive for food packaging (Jamróz et al., 2019; Neves et al., 2022; Velásquez et al., 2021). The visual perception of pH-dependent color change could also be facilitated by incorporating black elderberry into intelligent (smart) packaging (Neves et al., 2022). Çetinkaya et al. produced electrospinning gelatin nanofibers with black elderberry extract, Au nanoparticles, and SnO_2 to serve as color-changing indicators for fresh food (Cetinkaya et al., 2024). Also, the antioxidant capacity of black elderberry extract is considerable. It inhibits lipid oxidation and microbial growth (Jonušaite et al., 2021; Martínez-Hernández et al., 2024). Anti-inflammatory is another critical feature of elderberry (Crisan et al., 2013). Utilized an extract from European black elderberry fruit as a reducing agent in the green synthesis of stable silver nanoparticles. Their findings revealed the extract's promising anti-inflammatory properties, both in laboratory and animal studies (David et al., 2014).

Due to the potential side effects of synthetic compounds, substituting them with natural ones is necessary in biomedical and food packaging applications. This study aims to synthesize eco-friendly silver nanoparticles without harmful chemicals and incorporate them into electrospun fibers. Thyme and black elderberry were selected to facilitate the production of AgNPs. They characterized with i*n vitro* antibacterial analysis, and i*n vitro* cell studies as well as nanofiber properties and compared their performance.

2. Materials and methods

2.1. Preparation of thyme (Thymus vulgaris) extract

The plant extraction was prepared using thyme (*Thymus vulgaris*) grown in the Yalova-Altınova region in May 2023. The plant was first washed in tap water, removed from all dust, and rinsed with pure water. It was dried at room temperature to remove water from the leaf surfaces. After the washed and dried plants were ground, 10 g of plant material was placed in a 250 ml beaker containing 100 ml pure water and stirred with a magnetic stirrer for 40 minutes at 80°C. Then, it was stirred and cooled at room temperature (24°C) on a magnetic stirrer for 60 minutes. Plant extract was obtained by filtering plant waste from the solution with the help of a strainer. The plant extract was centrifuged at 4.000 rpm for 10 minutes to ensure that micro-sized impurities from the plant remained in the pellet. Finally, the supernatant was filtered with Whatman filter paper No.1 and stored at 4°C for further use.

2.2. Preparation of black elderberry (Sambucus nigra) extract

The plant material was obtained from the Bezmialem Phytotherapy and Education Application and Research Center (BİTEM). The plant was first washed in tap water, removed from all dust, and rinsed with pure water. It was dried at room temperature. Dried plants were ground, and 10 g of plant material was placed in a 250 ml beaker containing 100 ml of pure water and stirred with a magnetic stirrer for 30 minutes at 80°C. Then, it was stirred and cooled at room temperature (24°C) on a magnetic stirrer for 60 minutes. Plant extract was obtained by filtering plant waste from the solution with the help of a strainer. The plant extract was centrifuged at 4.000 rpm for 10 minutes to ensure that micro-sized impurities from the plant remained in the pellet. Finally, the supernatant was filtered with Whatman filter paper No.1 and stored at 4°C for further use.

2.3. Synthesis of silver nanoparticles using thyme (Thymus vulgaris) extract

To initiate the synthesis of AgNPs (Sigma Aldrich), 1 ml of thyme (*Thymus vulgaris*) extract was magnetically stirred with 19 ml of 1 mM $AgNO_3$ solution at 700 rpm at 45°C. The color of the reaction mixture

changed from green to dark brown, indicating that silver ions had transformed into silver nanoparticles. Then, the synthesized silver nanoparticles were centrifuged at 12.000 rpm at 4°C for 20 min. The obtained silver nanoparticles were washed using ultrapure water to eliminate all residues. Finally, the purified AgNPs were freeze-dried with a lyophilizer and then stored at 4°C.

2.4. Synthesis of silver nanoparticles using black elderberry (Sambucus nigra) extract

For silver nanoparticle synthesis from black elderberry (*Sambucus nigra*) extract, 1 ml of plant extract and 9 ml of 1 mM $AgNO_3$ were stirred with a magnetic stirrer at 700 rpm at 45°C. The color of the reaction mixture changed to dark brown, indicating that silver ions had transformed into silver nanoparticles. Then, the synthesized silver nanoparticles were centrifuged at 12.000 rpm at 4°C for 20 min. The obtained silver nanoparticles were washed using ultrapure water to eliminate all residues. Finally, the purified AgNPs were freeze-dried with a lyophilizer and then stored at 4°C.

2.5. Preparation of the Ag/Nanoparticle loaded PVA solutions and composite fibers

First, a solution of 10 % wt. polyvinyl alcohol (PVA) (Mw of 85000–124000, 99 % hydrolyzed, Sigma Aldrich) was prepared by dissolving in distilled water at 80°C for approximately 2 hours. Then, the magnetic stirrer was set at 450 rpm at room temperature for 24 hours. For electrospinning, a 10 ml syringe fitted with a steel needle was filled with the PVA solution, and the process was performed at a controlled 9 kV and a constant 5 ml/h flow rate. The collector was maintained at a steady 15 cm. The green synthesized 1 and 2 wt%. Ag from thyme and black elderberry nanoparticles were meticulously added to the room-temperature PVA solution and electrospun at the same electrospinning conditions.

2.6. UV-Vis analysis

The nanoparticles generated were first characterized by UV-Vis spectroscopy (UV 1900 Shimadzu, Japan). Throughout the synthesis, spectra were obtained at regular intervals between 200 and 800 nm in the wavelength range, with a resolution of 1 nm. Ultrapure water was used to dilute high-density samples to generate spectra with an absorbance of less than one.

2.7. Morphological analysis with SEM and TEM

Using a 200 kV Oxford Instruments X-Max 80 T Energy Dispersive Spectrometer (EDS) instrument and a JEOL JEM 2100 High-Resolution Transmission Electron Microscope (HRTEM) with a LaB6 filament, the morphology at the nanoscale was further examined. Copper TEM grids covered with carbon support film (Electron Microscopy Sciences, CF200-Cu, 200 mesh) were employed. The images were taken by the Gatan Model 833 Orius SC200D CCD Camera. The Gatan Microscopy Suite (GMS) 2 software and the Model 794 Slow Scan CCD Camera were used to record HRTEM images. CrystBox was used to index the diffraction patterns (Klinger and Jäger, 2015).

2.8. Chemical bond analysis with FTIR

To identify the chemical bonds in their structure, Fourier Transform Infrared (FTIR) spectra were obtained at 20 °C between 4000 and 400 cm^{-1}. Using an ATR (Attenuated Total Reflectance) unit on a Perkin Elmer spectrometer, the results were recorded in transmittance mode (T %). Four scans with a resolution of 4 cm^{-1} were carried out.

2.9. Thermal analysis

The thermal behavior of the samples was analyzed using the Differential Scanning Calorimeter (DSC). Analyzes were carried out at a heating rate of 10 °C/min, in the temperature range of 20–250°C, under continuous nitrogen gas flow using a Perkin-Elmer DSC 4000 device. The glass-transition temperature (T_g), melting temperatures (T_m), and enthalpy of melting (ΔH_m) of the samples were measured. The degree of crystallinity (X_c) was calculated using Eq. 1:

$$X_c = (\Delta H_m \times (\Delta H_m^0 \times \quad w)^{-1} \times 100 \tag{1}$$

where w is the weight fraction of PVA and ΔH_m^0 is the enthalpy of melting for 100 % crystalline PVA, which was taken as 138.6 J/g (Peppas and Merrill, 1976).

2.10. X-ray diffraction analyses

The X-ray Diffraction (XRD) analysis equipment Bruker 8 with Cu Kα radiation (λ = 1.54 Å) was used. The sample was positioned to cover an area 1 cm long and 3 mm wide using a metal sample holder. The sample holder was then employed inside and secured inside the equipment. The operation voltage and the current were settled as 40 kV and 30 mA, respectively. Tests were performed in the 2θ= 0–90° range with a 0.02° step size (Sharma et al., 2014).

2.11. In vitro antibacterial analysis

Bacterial studies were carried out in Fatih Sultan Mehmet Vakıf University Biomaterial Nanotechnology BİORGİNE Laboratory. Antimicrobial tests were performed using the Agar Disc Diffusion Assay method (Ciftci, 2024; Özdemir et al., 2024). *Gram-negative*: *Escherichia coli* (ATCC 25922) pathogen was tested. Nanoparticles were sterilized under UV for 2 hours and then placed on the agar surface on which bacteria were cultured with the help of a sterile clamp. During this process, a distance of 22 mm between the discs and 14 mm from the edge of the petri dish was taken into consideration in order to prevent the zones to be formed from overlapping each other. The media were then incubated at 37°C for 18–24 hours, and the inhibition zones were measured using calipers (Balouiri et al., 2016). Each nanoparticle material was measured ≤3 times, and the average value was expressed as zone growth.

2.12. In vitro cell study

Cell studies were conducted at the Fatih Sultan Mehmet Foundation University's BİORGİNE Biomaterials Nanotechnology Laboratory in compliance with ISO 10993–5 standards (CSA, 2009). The L929 cell line, sourced from ATCC, was used for in vitro experiments. The cells were cultured in Dulbecco's Modified Eagle Medium (DMEM/F12) from Sigma Aldrich, supplemented with fetal bovine serum (FBS) from the same company. Additional reagents, including penicillin-streptomycin antibiotic solution (GeneMark), trypsin-EDTA (0.25 %) and Trypan Blue (Gibco), phosphate-buffered saline (PBS) tablets, 2,3-bis-(2-methoxy-4-nitro-5-sulfenyl)-2H-tetrazolium-5-carboxylate (XTT) from Sigma Aldrich, and Phenazine Methosulfate (PMS) from Santa Cruz Biotechnology, were also utilized. The cells were maintained in DMEM/F12 medium, supplemented with 10 % FBS and penicillin-streptomycin (10,000 units/ml penicillin and 10 mg/ml streptomycin), and incubated at 37°C with 5 % CO_2. Upon reaching confluence, cells were detached using trypsin and centrifuged at 1000 rpm for 5 minutes (Narath et al., 2023). After removing the supernatant, the cells in the pellet were counted using a hemocytometer before proceeding with the cytotoxicity assay.

2.12.1. Indirect contact method

L929 cells were seeded in a 96-well plate at a density of 1×10^4 cells/well and incubated for 24 hours at 37°C in an atmosphere of 5 % CO_2 for cell attachment to the plate surface. For the biocompatibility examination of the fibers, the culture medium was removed, and the PVA/AgNPs fibers medium was added in varying dilutions (1:1, 1:2, 1:4 and 1:8) to the wells. Thyme and BE NPs was added to culture medium different concentration (25, 50, 75, and 100 µL). After 24-hour incubation, the medium was replaced with medium containing 0.1 % (v/v) PMS and 0.4 mg/ml XTT and incubated for another 4 hours at 37°C. The biocompatibility of the fibers was expressed as the percentage of cell viability calculated from the ratio between the number of cells treated with the fibers NPs and the untreated cells (control).

2.13. Statistical analysis

ANOVA and the GraphPad Prism program (GraphPad'8 Software Inc., San Diego, CA, USA) were utilized for the statistical analyses of the data. The statistical differences between the results, which were shown as means ± standard deviation (SD), were examined using one-way ANOVA and Tukey's multiple comparison tests. In each case, a value of $P < 0.0001$ was taken into consideration to establish statistical significance.

3. Result and discussion

3.1. Characterization results of green synthesized Ag NPs

Fig. 1 **a** and **b** show the UV-Vis spectrum of Thyme_AgNP and BE_AgNP, respectively. As is typical for AgNPs, the surface plasmon

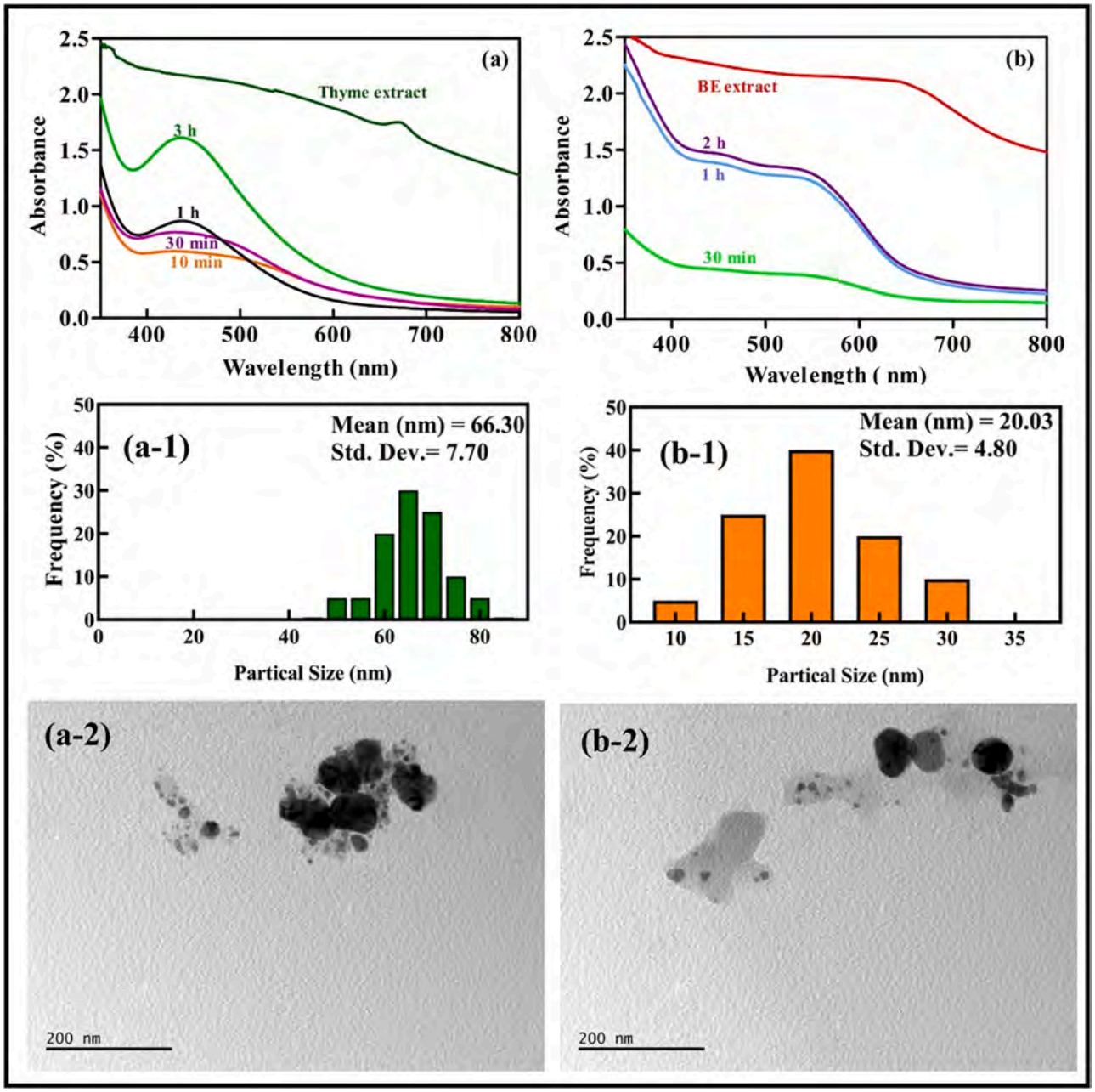

Fig. 1. Thyme_AgNPs, a) UV–Vis spectra, a-1) average particle size histogram, a-2) TEM images at a scale of 200 nm, and BE_AgNPs, b) UV–Vis spectra, b-1) average particle size histogram, b-2) TEM images at a scale of 200 nm.

resonance peaks ranged between 400 and 500 nm in length (Cavassin et al., 2015). Surface plasmon resonances are strongly influenced by metallic nanoparticles' dimensions, forms, and functionalization. A significant peak of around 450 nm in both spectra indicates that the AgNPs produced in the solution are approved, as seen in Fig. 1**a** and Fig. 1**b**(Coronado et al., 2011).

The synthesis of AgNP was suggested by the emergence of a yellowish-brown color caused by the activation of surface plasmon vibrations in the AgNPs (Opris et al., 2019).

The TEM image of Thyme_AgNPs is given in Fig. 1**a-2,** and the particle size histogram is illustrated in Fig. 1**a-1**. The average particle size of Thyme_AgNP was calculated as 66.30 ± 7.70 nm. BE_AgNPs particle size was measured as 20.03 ± 4.80 nm, and the TEM image is shown in Fig. 1**b-2**. These nanoparticles were synthesized according to their optimum conditions. The extract content remained constant; however, the $AgNO_3$ solution varied as 19 ml for Thyme and 9 ml for BE, which may have led to the variation between the particle sizes.

HRTEM investigations also helped to understand nanoparticle size, shape, and phase. In Fig. 2, a representative HRTEM study is shown for Ag nanoparticles. The HRTEM image and Fast Fourier Transformation (FFT) diffractogram are of BE_AgNPs. The HRTEM image labeled Fig. 2**c** is a magnified view of Fig. 2**b** showing (111) d-spacings of Ag.

3.2. Determination of structural, morphological properties of AgNP added PVA

10 wt% PVA electrospun at 9 kV voltage and a 5 ml/h flow rate and the SEM images of the obtained fibers are seen in Fig. 3**a-1, a-2**. The bead-free fiber formation was observed with a fiber diameter of around 400 nm. Various amounts of AgNPs, produced from thyme and black elderberry, were added into PVA solutions and electrospun. Fig. 3 **b and c** represent the fiber morphology image of PVA/Thyme. Additionally, in Fig. 3**d and e**, SEM and histograms of PVA/BE are shown. According to histogram analysis, all fiber diameters decreased with adding Ag nanoparticles. The average fiber diameter of PVA/Thyme was calculated at around 300 nm while PVA/BE was 200 nm. Many factors commonly subdivide solution, process, and environment affect fiber morphological attitude. Solution characteristics such as viscosity, conductivity, surface tension, etc., influence diameter more (Casasola et al., 2014; Celebioglu et al., 2014; Chen et al., 2007; Duygulu et al., 2020; Ebrahimi and Ramezani Dana, 2022). The fiber diameter and morphology of the fibers are affected by various factors, especially the physical properties of the solvent, such as boiling point, viscosity, and conductivity (Celebioglu et al., 2014; Duygulu et al., 2020).

The statistical analysis results demonstrated an apparent influence of Ag NP addition on the fiber diameter of PVA nanofiber ($P < 0.0001$). As shown in Fig. 3, the calculated fiber diameters were 397.76 ± 88.40, 332.95 ± 86.37, 316.07 ± 68.53, 220.32 ± 46.74, and 245.63 ± 69.84 nm for PVA, PVA / Thyme_1, PVA / Thyme_2, PVA / BE_1, and PVA / BE_2, respectively. The average fiber diameter generally decreased with the addition of AgNP's. Wang et al. (Wang et al., 2012) also added Ag nanoparticles into polyacrylonitrile, and they observed that when Ag is added, the charge density of the solution rises, causing the ejected jets with strong elongation forces in the electrical field and producing thinner composite fibers.

It's important to note that the additional amount of Thyme did not

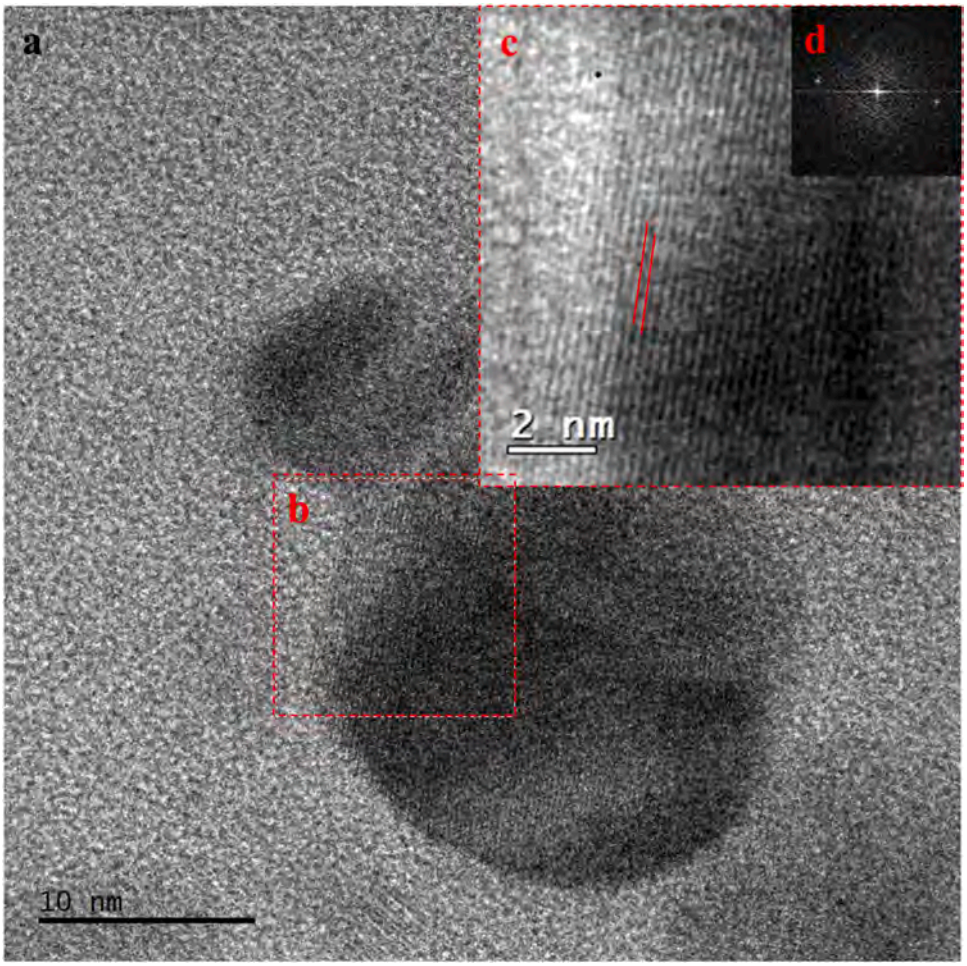

Fig. 2. a) HRTEM image and FFT diffractogram of BE_AgNPs. HRTEM image labeled c) is a magnified view of b) showing (111) d-spacings of AgNP.

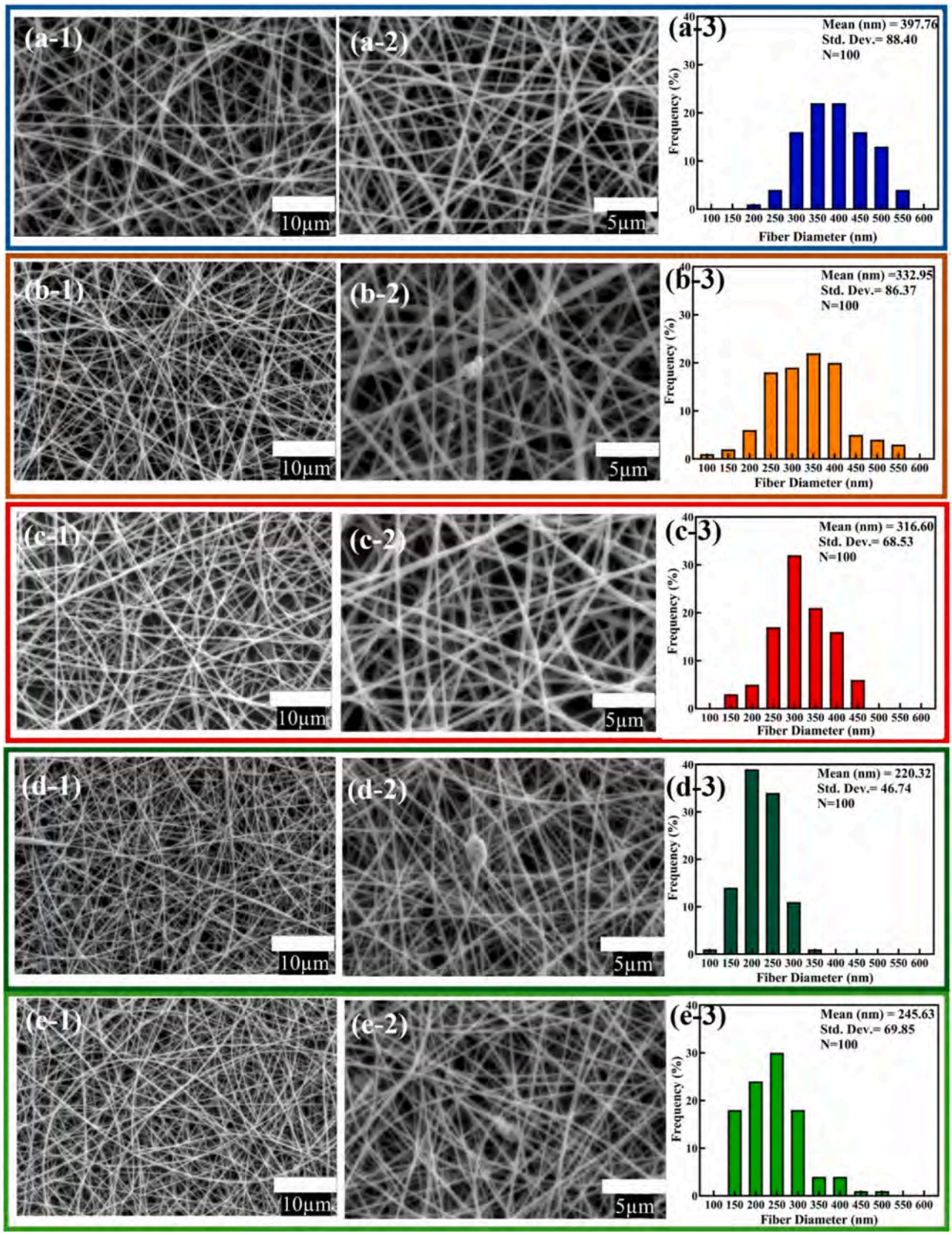

Fig. 3. SEM analysis of a) PVA, b) PVA/Thyme_1, c) PVA/Thyme_2, d) PVA/BE_ 1, e) PVA/BE_2.

result in a significant difference, while the variation in BE did influence the fiber diameter. The decline in the average fiber diameter compared between PVA nanofiber and the Ag nanoparticles synthesized from Thyme extract measured around %20, while for BE extract, it was calculated at nearly %40. Additionally, the low standard deviation values of the fibers provide homogeneous fiber distribution. In the current study, the Ag NP content and synthesis material varied while all the conditions remained constant. The particle diameter of Thyme measured around at approximately 70 nm, while black elderberry was calculated at nearly 20 nm. The measured fiber diameter indicated that the smaller particle diameter led to a thinner fiber diameter. This can be attributed to the small size of NPs dispersed in the PVA fiber better, the increased electrical stretch on the polymer solution, and the charge repulsion of the polymer jet. Furthermore, the research by Zhang et al. (2016) revealed that an increase in AgNPs leads to improved electrostatic stress, causing the droplets from the Taylor cone to stretch quickly and form fibers with smaller diameters, thereby demonstrating the practical relevance of our findings.

Fig. 4 provides the threshold of the SEM images displayed in Fig. 3. According to fiber thresholding used for Image J porosity analysis, Table 1 shows the porosity percentage results. The porosity of the nanofibers decreased generally with the addition of Ag NPs, a finding that has practical implications for nanofiber applications. When the porosity percentages are compared to PVA nanofibers, %56.94, 54.45, 40.57, and 38.43 for PVA/Thyme_1, PVA/Thyme_2, PVA/BE_1, and PVA/BE_2, respectively increment was observed.

Many factors commonly subdivide solution, process, and environment affect fiber morphological attitude. More factors affect diameter, including surface tension, conductivity, and viscosity of the solution. Our objective in this study is to investigate the effects of varying AgNP content and synthesis material on the morphological characteristics of nanofibers. TEM images of nanofibers with silver nanoparticle-added are displayed in Fig. 5. All Ag nanoparticles disperse homogeneously inside PVA fibers; no protrude occurrence was observed. Saquing et al. (2009) investigated the presence of synthesized AgNP in electrospun polymer nanofibers. At greater Ag concentrations, they observed several AgNPs protruding on the nanofiber surface. They explain this situation as different electrical field effects on the polymer and metal nanoparticles, which have varying electrical conductivity and polarizability.

3.3. FTIR

Fig. 6 shows the FTIR spectra of PVA, PVA/Thyme_1, PVA/Thyme_2, PVA/BE_1, PVA/BE_2 nanofibers. The Ag-PVA spectrum is attributed to stretching vibrations at 3358 (O-H) cm^{-1} (Al-Bermany et al., 2023;

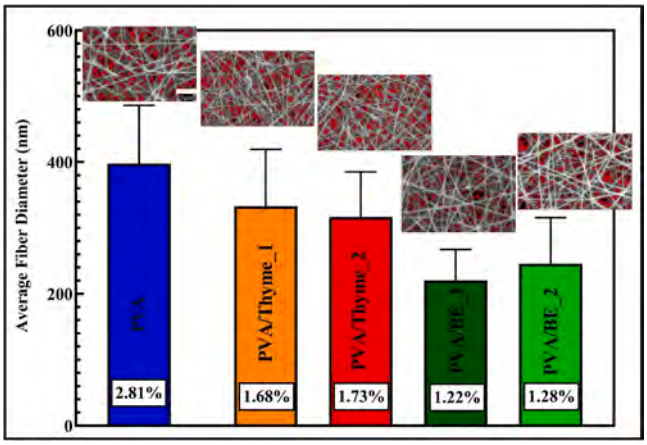

Fig. 4. The variation in average fiber diameters, porosity percentages, and thresholding of PVA, PVA/Thyme_1, PVA/Thyme_2, PVA/BE_1, PVA/BE_2 nanofibers.

Table 1
Sample code, average fiber size, porosity and average pore area of the nanofibers.

Sample code	Fiber diameter (nm)	Average Fiber Area (μm^2)	Porosity (%)
PVA	397.76 ± 88.40	6503	2.81
PVA/Thyme_1	332.95 ± 86.37[a]	6842	1.21
PVA/Thyme_2	316.07 ± 68.53[a]	6599	1.28
PVA/BE_1	220.32 ± 46.74[a]	6761	1.67
PVA/BE_2	245.63 ± 69.84[a]	6638	1.73

[a] Statistical significance level determined as ($P < 0.0001$), and the parenthesis indicates standard deviation.

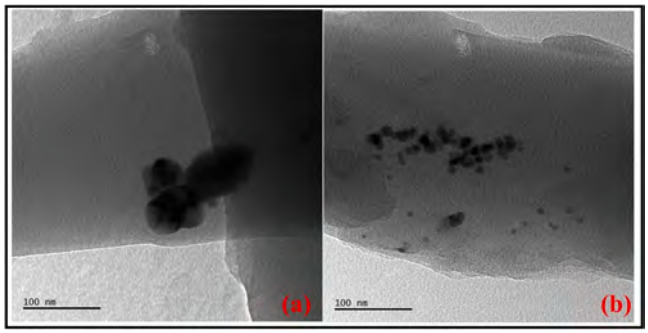

Fig. 5. TEM images of nanofibers: a) PVA/Thyme, b) PVA/BE.

Mejía Suaza et al., 2023) associated with strong intramolecular and intermolecular hydrogen bonding. Simultaneously, we observe a notable enlargement and weakening of the stretching modes 3320 cm^{-1} (O-H) (David et al., 2014; Moldovan et al., 2016) due to the decrease in the number of OH groups due to the esterification reaction. The intensity of the band belonging to C═O stretching vibrations observed at 1729 cm^{-1} in PVA increased significantly in PVA/BE_1 (1721 cm^{-1}) and PVA/Thyme_2 (1729 cm^{-1}) (Al-Jahani, 2021; Mirsharifi et al., 2023). Once more, the band belonging to C-N stretching vibrations observed at 1086 cm^{-1} in PVA shifted to 1255 cm^{-1} for PVA/Thyme_2 and 1247 cm^{-1} for PVA/BE_1, and the intensity of the peaks increased. Although the C-O stretching bands were observed at 1086 cm^{-1} for each sample, the peak intensities of PVA/Thyme_2 and PVA/BE_1 increased compared to PVA. When looking at the spectra, C-H bending vibrations were observed at 845 cm^{-1} for PVA, 842 cm^{-1} for PVA/BE_1, and 838 cm^{-1} for PVA/Thyme_2. These small differences suggest that AgNPs synthesized with plant extracts physically interact with PVA. The significant changes in the spectra of PVA/Thyme_2 and PVA/BE_1 indicate that Thyme-AgNPs and BE_AgNPs synthesized using thyme and black elderberry extracts interact with the PVA matrix.

3.4. Thermal analysis

Differential scanning calorimeter curves of neat PVA nanofibers and nanofibers with additives were reported in Fig. 7. All curves showed two endothermic peaks during the heating. Due to the high hydrophilicity of PVA, it keeps high amounts of free water, and this water evaporates during heating (Costa et al., 2013). Thus, the evaporation of the free water possibly leads to the first larger peaks in the DSC curves. Also, the first peaks of nanofibers with additives shifted to lower temperatures with lower intensities. This could result from more evaporation in PVA nanofibers without additives, possibly because additives had less water content than PVA.

The second endothermic peaks in DSC curves, observed at around 195°C, signify the melting of PVA. The data from the DSC, presented in Table 2, reveal that the introduction of additives has diverse effects on PVA's thermal behaviors. In general, additives have increased both the

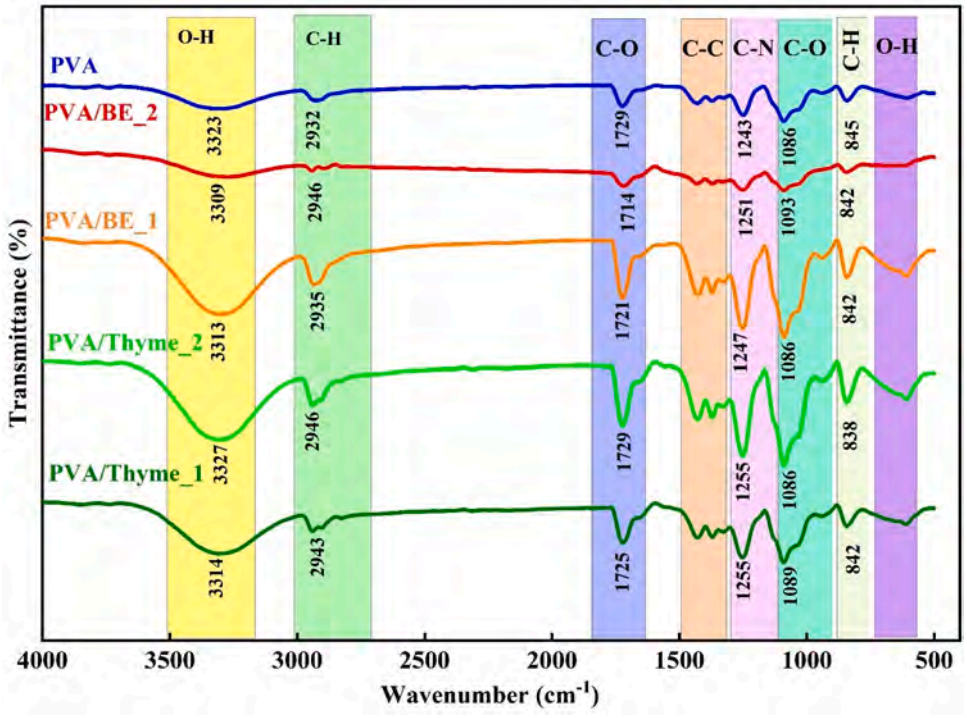

Fig. 6. FTIR structures PVA, PVA/Thyme_1, PVA/Thyme_2, PVA/BE_1, PVA/BE_2 nanofibers.

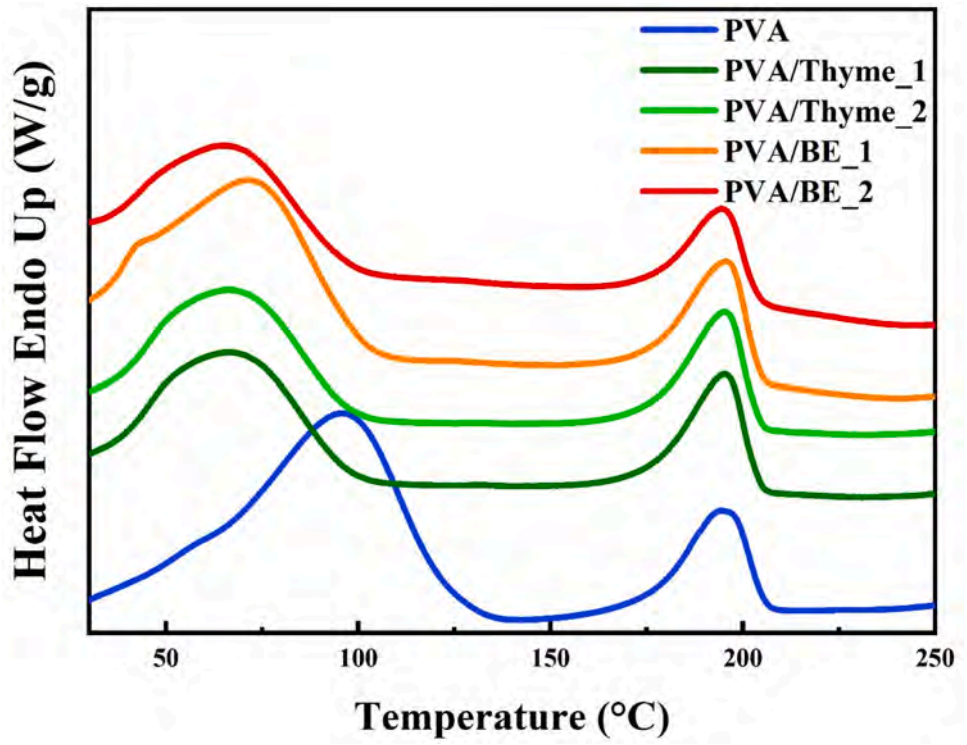

Fig. 7. DSC thermograms of PVA nanofibers and PVA nanofibers with thyme and black elderberry at 1 and 2 % content.

glass transition and melting temperatures compared to neat PVA nanofibers. However, the content of additives has led to different outcomes. An increase in thyme content has slightly raised the temperatures, while an increase in black elderberry content has caused a decrease in temperatures.

The degree of crystallinity is the energy required to melt a certain number of crystals in polymer. X_c was 29.96 % for the neat PVA nanofibers. Both thyme and black elderberry addition at 1 wt% increased X_c values of the nanofibers. In thyme added nanofibers, increasing thyme concentration to 2 % significantly increased the X_c. Although black elderberry addition at 1 wt% concentration induced more X_c than 1 wt% thyme added counterpart, increasing amount of black elderberry caused decreased in X_c. The nanoparticles may function as nucleating agents and initiate crystallinity by forming a large number

Table 2
DSC data of the PVA and PVA with AgNP additives.

Sample code	T_g (°C)	T_m (°C)	ΔH_m (J/g)	Xc (%)
PVA	68.03	193.79	41.53	29.96
PVA/Thyme_1	70.29	195.25	42.69	34.32
PVA/Thyme_2	70.32	195.36	42.35	38.19
PVA/BE_1	70.12	195.88	45.57	36.53
PVA/BE_2	69.92	194.93	33.06	29.82

of crystal nuclei. Here, both additives improved crystallinity, possibly by acting as nucleating agents. Especially, further crystallization behavior promoted with the increasing amount of thyme. On the other hand, the increase in the concentration of black elderberry prohibited crystallization and even resulted in an Xc value that was lower than neat nanofabric.

3.5. XRD

Fig. 8 exhibits the XRD patterns of Ag NPs added PVA nanofibers. The polyvinyl alcohol fibers exhibit a semicrystalline character and a noticeable peak around 2θ= 29.4°, which belongs to (101), and the peak is seen in all nanofibers.

For all fiber samples, the highly intense peaks are generally observed for (220) and (311) reflections. Table 3 presents the standard diffraction angle (2θ) and the experimentally obtained X-ray diffraction angle (2θ)

Table 3
Position and crystallite sizes of (002) and (311) for PVA/Thyme_1, PVA/Thyme_2, PVA/BE_ 1, PVA/BE_ 2.

Sample code	Position of (002) 2θ (°)	(002) Crystallite Size (nm)	Position of (311) 2θ (°)	(311) Crystallite Size (nm)
JCPDS silver:89–3722	64.45		77.41	
PVA/Thyme_1	65.47	75.35	78.55	92.53
PVA/Thyme_2	65.24	11527	78.48	96.75
PVA/BE_1	65.44	106.02	78.57	78.41
PVA/BE_2	65.37	107.19	78.36	100.87

of silver particles. The data for the particles were provided by the standard powder diffraction card of JCPDS, silver PDF Number 89–722. The crystallite sizes measured by using the Debye-Scherrer formula showed variations. According to the TEM image in Fig. 5, the AgNPs were placed inside the fiber and dispersed homogeneously; however, some clutter formation of the NPs may influence the peak intensity and the crystallite size.

TEM-EDS helps to determine that the majority of the nanoparticles are Ag (Fig. 9). Selected area electron diffraction (TEM-SAED) pattern indexation also matches the major (hkl) planes of the Ag phase, as shown in Fig. 9.

The standard powder diffraction card of the JCPDS silver file is compared to the XRD pattern of the electrospun AgNPs, adding PVA

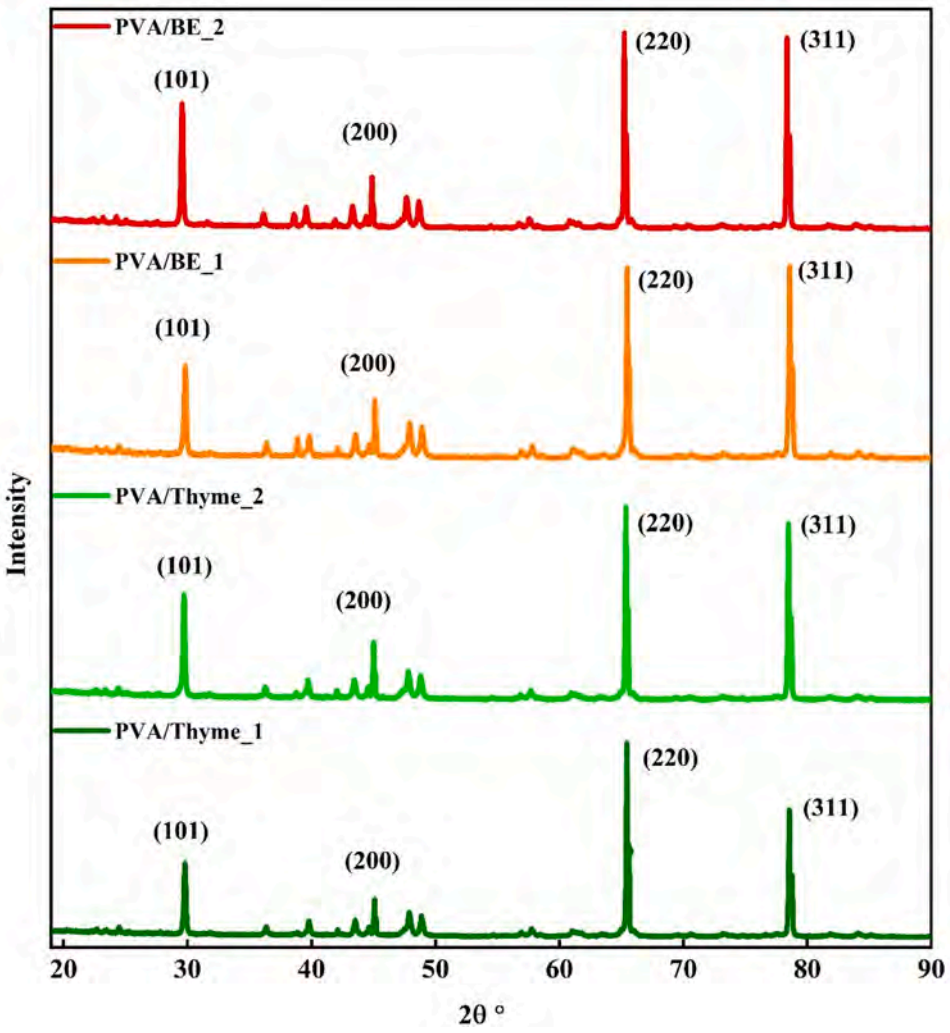

Fig. 8. XRD of PVA/Thyme_1, PVA/Thyme_2, PVA/BE_1, PVA/BE_2 nanofibers.

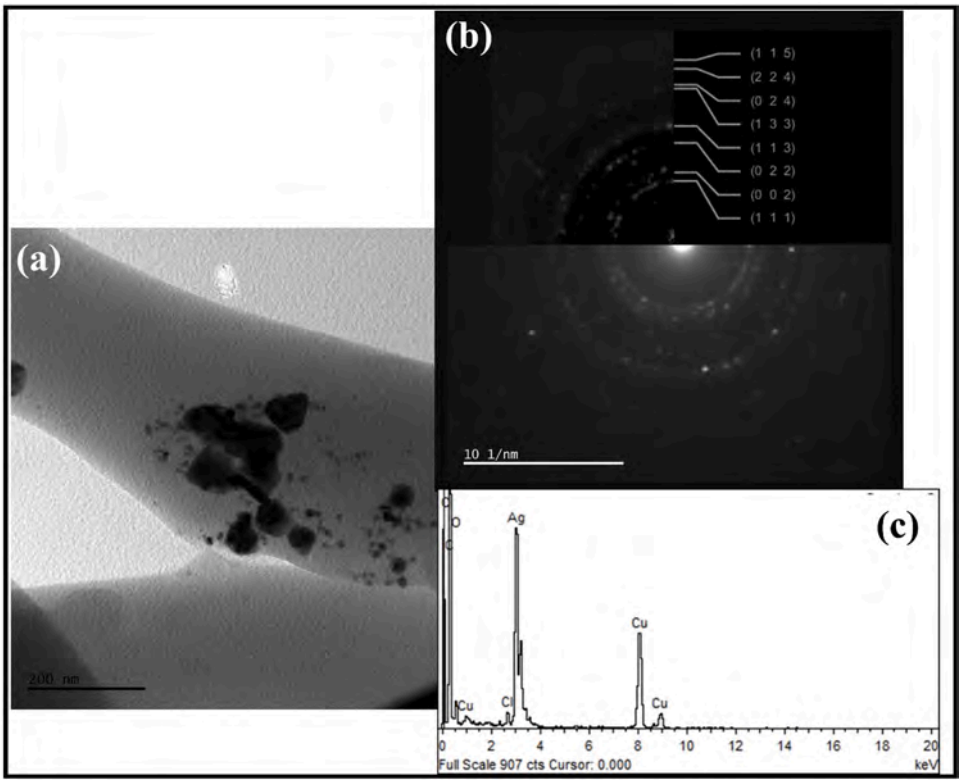

Fig. 9. Ag nanoparticles a) TEM image b) Selected area electron diffraction (SAED) pattern and indexation results c) TEM-EDS spectrum of PVA/BE_1 nanofiber.

nanofibers. The peaks have been determined to coincide with the levels of silver (hkl). The XRD analysis verifies that the end products are FCC-structured silver nanoparticles.

3.6. *In vitro antibacterials*

The Disc Diffusion Assay method is employed to investigate the responses of PVA, PVA/Thyme_2, and PVA/BE_1 nanofibers against *E. coli*,

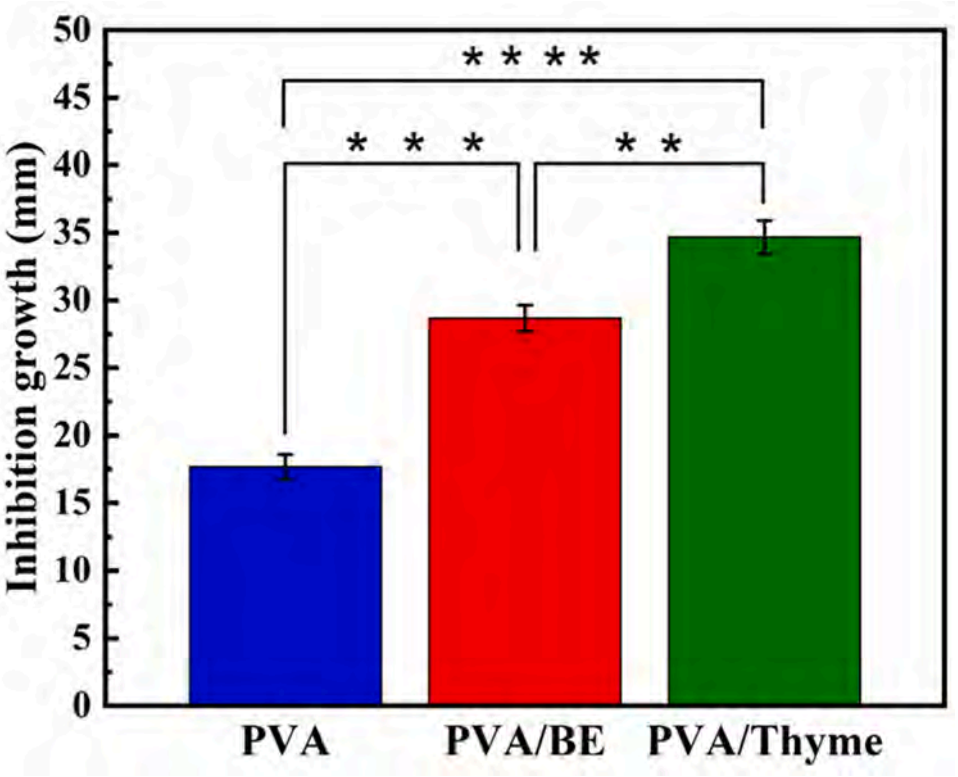

Fig. 10. *E. coli* inhibition growth of the PVA and PVA with AgNP additives. (Statistical significance level determined as ($P < 0.0001$)).

revealing their potential antibacterial activities. PVA nanofiber serves as our control group. Fig. 10 illustrates the antibacterial activities of the nanofibers against *E. coli*, and the inhibition zone diameters were calculated as 17.67 ± 0.91 mm, 28.66 ± 0.95 mm, and 34.67 ± 1.25 mm for PVA, PVA/Thyme, and PVA/BE, respectively. These results revealed that both Thyme and BE show antibacterial properties, and among them, PVA/Thyme nanofiber exhibited the highest inhibition growth against *E. coli.*

In a similar study, a cream containing BE, colloidal nanosilver (AgNPs), was designed, and its antimicrobial effect was investigated *in vitro*. *E. coli, S. aureus*, and *C. albicans* were selected as pathogens. The agar-gel diffusion method and suspension tests were used to determine the duration of antimicrobial activity of the designed BE_AgNP cream. The tested Gram-negative microorganisms died in a much shorter time than Gram-positive ones. The highest sensitivity was found in *E. coli* (Popova et al., 2022). Aldosary et al. (Aldosary et al., 2023) synthesized *Thymus vulgaris* silver nanoparticles (TAgNPs), and compared the antimicrobial activities (*E. coli* ATCC 25922) of TAgNPS and *Thymus vulgaris* essential oil extract. TAgNPs showed significantly higher antimicrobial activity than Thymus and other thymus formulations, demonstrating their potential in antimicrobial applications. Also, green silver nanoparticles were synthesized using essential oils of thyme (*Origanum vulgare*), oregano (*Thymus vulgaris*), clove (*Syzygium aromaticum L.*), rosemary (*Rosmarinus officinalis L.*) and *Poiretia latifolia* for use in food packaging applications. The developed silver nanoparticles showed antimicrobial activity against *Staphylococcus aureus* at different concentrations (40–100 μL ml^{-1}) (Vinicius de Oliveira Brisola Maciel et al., 2020). In another green synthesis study, the synthesis of silver nanoparticles was developed using *Thymus vulgaris*, *Mentha piperita* and *Zingiber officinale* extracts. *Acinetobacter baumannii*, *Staphylococcus aureus*, and *Escherichia coli* were the targets of different degrees of inhibition zones shown by the antibacterial qualities of AgNPs extracts using the agar well diffusion method. The green synthesized AgNPs demonstrated strong antibacterial activity against four multidrug-resistant clinical isolates: *Escherichia coli*, *Acinetobacter baumannii*, and *Staphylococcus aureus* (Abdellatif et al., 2022).

3.7. Evaluation of biocompatility and bioactivity of NPs added PVA

Fig. 11**a** represents the effect of the fibers on L929 cell viability investigated using the direct contact method. AgNPs added PVA nanofibers did not demonstrate any cytotoxic impact according to ISO 10993–5 requirements. When L929 cell viability was examined by the indirect method, PVA/Thyme and PVA/BE nanofibers also did not show any toxic effect on the cells at any volume value. However, the rise in volume ratio caused a drop in cell viability for all fibers.

Generally, low concentrations are used to minimize the toxic effects of AgNPs on biological systems. These concentrations are important factors affecting the level of cytotoxicity of cells. As the concentration of AgNPs increases, cytotoxicity tends to increase (Cai et al., 2023; Li et al., 2020). Fig. 11**b** and **c** reveal that when the cell concentration increased (>50 μL), the cellular viability decreased in PVA/Thyme and PVA/BE nanofibers. As the concentration of cells decreased (< 50 μL), cell viability was 80 % and above. Better cell viability was observed in 0–25–50 μL concentrations for PVA/Thyme and PVA/BE nanofibers.

Similar studies evaluated the cell cytotoxicity of green synthesized Ag NPs fortified with thyme and ginger extracts on a human dermal fibroblast cell line based on an MTT assay. The results of Mohammadi et al. (2019) reveal that AgNPs synthesized with ginger extract are toxic at concentrations above 1.25 ppm. However, AgNPs synthesized with thyme extract did not show a cytotoxicity effect below a concentration of 3.5 ppm. In another study on silver nanoparticles/Thymus Kotschyanus extract, cells treated with different concentrations of silver nanoparticles (0, 25, 50, 100, and 200 μg/ml) were examined for cytotoxicity effect on Hela NCBI-C115 cells by MTT assay for 48 hours. Absorbance at 570 nm was measured and showed excellent viability up to 200 μg/ml (Hamelian et al., 2018). Moreover, David et al. (2014) biosynthesized AgNps from BE and Adoxaceae family, and they observed the anti-inflammatory effects on AgNPs through the reduction of cytokine production induced by UVB irradiation.

4. Conclusion

In this study, AgNPs were produced from Thyme and BE extracts

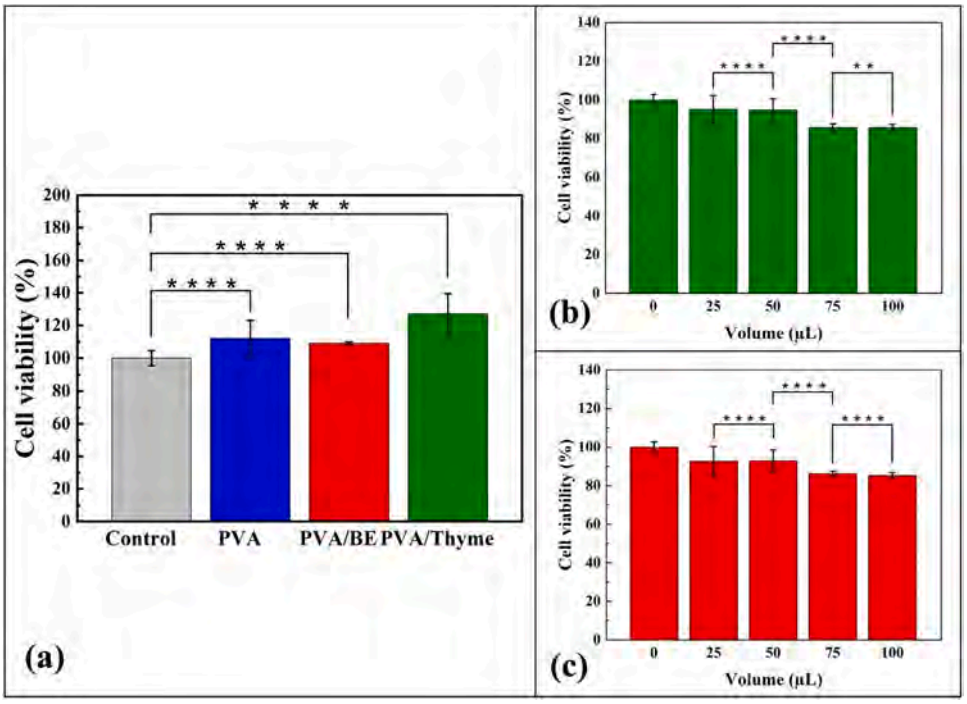

Fig. 11. a) XTT cytotoxicity analyses by direct contact method, b) and c) L929 cell viability of NPs by indirect contact method. (Statistical significance level determined as (P < 0.0001)).

using a low-cost, environmentally friendly green synthesis method. According to UV-Vis analysis, the absorbance peaks at 450 nm were found in both spectra, indicating that the AgNPs were obtained from extracts. Also, (111) d-spacing confirmed the presence of AgNPs in HRTEM observations. The average AgNP sizes were calculated around 66 and 20 nm for Thyme_AgNPs and BE_AgNPs, respectively. 1 and 2 wt % content of the AgNPs were added into the PVA solution, and electrospun, homogeneous fiber formations were observed with SEM and TEM. Characterization analyses, such as FTIR and DSC, revealed that PVA/Thyme_2 and PVA/BE_1 nanofibers showed better interactions within the nanofibers. The 2θ positions of the nanofibers obtained from XRD and the HRTEM demonstrated the presence of AgNPs in PVA nanofibers in the FCC structure. The antibacterial activity of Thyme and BE nanoparticles added nanofibers was evaluated against *E. coli*. PVA/Thyme nanofiber exhibited the largest inhibition growth.

Furthermore, *in vitro* biocompatibility studies, such as cell XTT cytotoxicity tests, revealed that PVA/Thyme performed better. This study can be considered an important step in the development of a promising new biomaterial for the future of nanotechnology. In this context, PVA/Thyme, with its high antimicrobial properties, offers great potential for tissue engineering, the food industry, biomedical applications, and non-toxic biomaterial.

Ethical approval

Not applicable

Declaration of AI and AI-assisted technologies in the writing process

During the preparation of this work the authors used chatGPT, quillbot, and grammarly in order to check grammar and increase readability. After using this tool/service, the authors reviewed and edited the content as needed and take full responsibility for the content of the publication.

CRediT authorship contribution statement

Aylin Altinbay: Writing – review & editing, Writing – original draft, Visualization, Validation, Resources, Project administration, Methodology, Funding acquisition, Formal analysis, Data curation. **Nilüfer Evcimen Duygulu:** Writing – review & editing, Writing – original draft, Visualization, Validation, Software, Resources, Methodology, Investigation, Formal analysis, Data curation. **Özlem Tavukcuoglu:** Writing – review & editing, Writing – original draft, Visualization, Validation, Software, Resources, Methodology, Investigation, Formal analysis, Data curation. **Fatih Ciftci:** Writing – review & editing, Writing – original draft, Visualization, Validation, Software, Resources, Methodology, Investigation, Formal analysis, Data curation.

Declaration of Competing Interest

The authors declare that they have no known competing financial interests or personal relationships that could have appeared to influence the work reported in this paper.

Acknowledgements

This work was supported by the Scientific and Technological Research Council of Turkey (TUBITAK) for the project with the identification number 121C440.

Data Availability

Data will be made available on request.

References

Abdellatif, A.A.H., Alhathloul, S.S., Aljohani, A.S.M., Maswadeh, H., Abdallah, E.M., Hamid Musa, K., El Hamd, M.A., 2022. Green synthesis of silver nanoparticles incorporated aromatherapies utilized for their antioxidant and antimicrobial activities against some clinical bacterial isolates. Bioinorg. Chem. Appl. 2022. https://doi.org/10.1155/2022/2432758.

Alayande, S.O., Akinsiku, A.A., Akinsipo (Oyelaja), O.B., Ogunjinmi, E.O., Dare, E.O., 2021. Green synthesized silver nanoparticles and their therapeutic applications. Comprehensive Analytical Chemistry, pp. 585–611. https://doi.org/10.1016/bs.coac.2021.01.009.

Al-Bermany, E., Mekhalif, A.T., Banimuslem, H.A., Abdali, K., Sabri, M.M., 2023. Effect of green synthesis bimetallic Ag@SiO2 core–shell nanoparticles on absorption behavior and electrical properties of PVA-PEO nanocomposites for optoelectronic applications. Silicon 15, 4095–4107. https://doi.org/10.1007/s12633-023-02332-7.

Aldosary, S.K., El-Rahman, S.N.A., Al-Jameel, S.S., Alromihi, N.M., 2023. Antioxidant and antimicrobial activities of Thymus vulgaris essential oil contained and synthesis thymus (Vulgaris) silver nanoparticles. Braz. J. Biol. 83. https://doi.org/10.1590/1519-6984.244675.

Al-Jahani, G.M.A.M., 2021. Thymus vulgaris (Thyme) as a natural organic matter to biosynthesis silver nanoparticles and their antibacterial efficiency. Int. J. Pharm. Res. Allied Sci. 10, 118–121. https://doi.org/10.51847/obv07gpj5c.

Ananda, A.P., Manukumar, H.M., Umesha, S., Soumya, G., Priyanka, D., Mohan Kumar, A.S., Krishnamurthy, N.B., Savitha, K.R., 2017. A relook at food packaging for cost effective by incorporation of novel technologies. J. Packag. Technol. Res. 1, 67–85. https://doi.org/10.1007/s41783-017-0011-4.

Balouiri, M., Sadiki, M., Ibnsouda, S.K., 2016. Methods for in vitro evaluating antimicrobial activity: a review. J. Pharm. Anal. https://doi.org/10.1016/j.jpha.2015.11.005.

Bao, N., Wei, Z., Ma, Z., Liu, F., Yin, G., 2010. Si-doped mesoporous TiO2 continuous fibers: preparation by centrifugal spinning and photocatalytic properties. J. Hazard. Mater. 174, 129–136. https://doi.org/10.1016/j.jhazmat.2009.09.026.

Bhattacharya, R., Mukherjee, P., 2008. Biological properties of "naked" metal nanoparticles. Adv. Drug Deliv. Rev. https://doi.org/10.1016/j.addr.2008.03.013.

Boskovic, M., Zdravkovic, N., Ivanovic, J., Janjic, J., Djordjevic, J., Starcevic, M., Baltic, M.Z., 2015. Antimicrobial activity of Thyme (Tymus vulgaris) and Oregano (Origanum vulgare) essential oils against some food-borne microorganisms. Procedia Food Sci. 5, 18–21. https://doi.org/10.1016/j.profoo.2015.09.005.

Cai, L., Zhu, X., Ruan, H., Yang, J., Wei, W., Wu, Y., Zhou, L., Jiang, H., Ji, M., Chen, J., 2023. Curcumin-stabilized silver nanoparticles encapsulated in biocompatible electrospun nanofibrous scaffold for sustained eradication of drug-resistant bacteria. J. Hazard. Mater. 452. https://doi.org/10.1016/j.jhazmat.2023.131290.

Casasola, R., Thomas, N.L., Trybala, A., Georgiadou, S., 2014. Electrospun poly lactic acid (PLA) fibres: effect of different solvent systems on fibre morphology and diameter. Polymer. https://doi.org/10.1016/j.polymer.2014.06.032.

Cavassin, E.D., de Figueiredo, L.F.P., Otoch, J.P., Seckler, M.M., de Oliveira, R.A., Franco, F.F., Marangoni, V.S., Zucolotto, V., Levin, A.S.S., Costa, S.F., 2015. Comparison of methods to detect the in vitro activity of silver nanoparticles (AgNP) against multidrug resistant bacteria. J. Nanobiotechnol. 13. https://doi.org/10.1186/s12951-015-0120-6.

Celebioglu, A., Aytac, Z., Umu, O.C.O., Dana, A., Tekinay, T., Uyar, T., 2014. One-step synthesis of size-tunable Ag nanoparticles incorporated in electrospun PVA/cyclodextrin nanofibers. Carbohydr. Polym. 99, 808–816. https://doi.org/10.1016/j.carbpol.2013.08.097.

Cetinkaya, T., Bildik, F., Altay, F., Ceylan, Z., 2024. Gelatin nanofibers with black elderberry, Au nanoparticles and SnO2 as intelligent packaging layer used for monitoring freshness of Hake fish. Food Chem. 437. https://doi.org/10.1016/j.foodchem.2023.137843.

Chen, C., Lv, G., Pan, C., Song, M., Wu, C., Guo, D., Wang, X., Chen, B., Gu, Z., 2007. Poly (lactic acid) (PLA) based nanocomposites - a novel way of drug-releasing. Biomed. Mater. https://doi.org/10.1088/1748-6041/2/4/L01.

Ciftci, F., 2024. Bioadhesion, antimicrobial activity, and biocompatibility evaluation bacterial cellulose based silver nanoparticle bioactive composite films. Process Biochem. 137, 99–110. https://doi.org/10.1016/J.PROCBIO.2023.12.021.

Coronado, E.A., Encina, E.R., Stefani, F.D., 2011. Optical properties of metallic nanoparticles: manipulating light, heat and forces at the nanoscale. Nanoscale 3, 4042–4059. https://doi.org/10.1039/c1nr10788g.

Costa, R.G.F., Ribeiro, C., Mattoso, L.H.C., 2013. Study of the effect of rutile/anatase TiO2 nanoparticles synthesized by hydrothermal route in electrospun PVA/TiO2 nanocomposites. J. Appl. Polym. Sci. 127, 4463–4469. https://doi.org/10.1002/app.38031.

Crisan, M., David, L., Moldovan, B., Vulcu, A., Dreve, S., Perde-Schrepler, M., Tatomir, C., Filip, A.G., Bolfa, P., Achim, M., Chiorean, I., Kacso, I., Grosan, C.B., Olenic, L., 2013. New nanomaterials for the improvement of psoriatic lesions. J. Mater. Chem. B 1, 3152–3158. https://doi.org/10.1039/c3tb20476f.

CSA, C.S.A., 2009. ISO 10993-5 in vitro cytotoxicity. Int. Organ. 1–11.

David, L., Moldovan, B., Vulcu, A., Olenic, L., Perde-Schrepler, M., Fischer-Fodor, E., Florea, A., Crisan, M., Chiorean, I., Clichici, S., Filip, G.A., 2014. Green synthesis, characterization and anti-inflammatory activity of silver nanoparticles using European black elderberry fruits extract. Colloids Surf. B Biointerfaces 122, 767–777. https://doi.org/10.1016/j.colsurfb.2014.08.018.

De Melo, A.P.Z., De Oliveira Brisola MacIel, M.V., Sganzerla, W.G., Da Rosa Almeida, A., De Armas, R.D., MacHado, M.H., Da Rosa, C.G., Nunes, M.R., Bertoldi, F.C., Barreto, P.L.M., 2020. Antibacterial activity, morphology, and physicochemical stability of biosynthesized silver nanoparticles using thyme (Thymus vulgaris) essential oil. Mater. Res. Express 7. https://doi.org/10.1088/2053-1591/ab6c63.

Dutta, N.K., Mazumdar, K., Gordy, J.T., 2020. The nucleocapsid protein of SARS–CoV-2: a target for vaccine development. J. Virol. https://doi.org/10.1128/jvi.00647-20.
Duygulu, N.E., Ciftci, F., Ustundag, C.B., 2020. Electrospun drug blended poly(lactic acid) (PLA) nanofibers and their antimicrobial activities. J. Polym. Res. https://doi.org/10.1007/s10965-020-02215-0.
Ebrahimi, F., Ramezani Dana, H., 2022. Poly lactic acid (PLA) polymers: from properties to biomedical applications. Int. J. Polym. Mater. Polym. Biomater. https://doi.org/10.1080/00914037.2021.1944140.
El-Desoky, M.M., Morad, I., Wasfy, M.H., Mansour, A.F., 2020. Synthesis, structural and electrical properties of PVA/TiO2 nanocomposite films with different TiO2 phases prepared by sol–gel technique. J. Mater. Sci. Mater. Electron. 31, 17574–17584. https://doi.org/10.1007/s10854-020-04313-7.
Güneş Çimen, C., Dündar, M.A., Demirel Kars, M., Avcl, A., 2022. Enhancement of PCL/PLA electrospun nanocomposite fibers comprising silver nanoparticles encapsulated with Thymus vulgaris L. molecules for antibacterial and anticancer activities. ACS Biomater. Sci. Eng. 8, 3717–3732. https://doi.org/10.1021/acsbiomaterials.2c00611.
Hamelian, M., Zangeneh, M.M., Amisama, A., Varmira, K., Veisi, H., 2018. Green synthesis of silver nanoparticles using Thymus kotschyanus extract and evaluation of their antioxidant, antibacterial and cytotoxic effects. Appl. Organomet. Chem. 32. https://doi.org/10.1002/aoc.4458.
Hosseinzadeh, E., Foroumadi, A., Firoozpour, L., 2023. What is the role of phytochemical compounds as capping agents for the inhibition of aggregation in the green synthesis of metal oxide nanoparticles? A DFT molecular level response. Inorg. Chem. Commun. 147. https://doi.org/10.1016/j.inoche.2022.110243.
Ingram Taylor, G., 1969. Electrically driven jets. Proc. Roy. Soc. Lond. A. 313, 453–475. https://doi.org/10.1098/rspa.1969.0205.
Jamkhande, P.G., Ghule, N.W., Bamer, A.H., Kalaskar, M.G., 2019. Metal nanoparticles synthesis: an overview on methods of preparation, advantages and disadvantages, and applications. J. Drug Deliv. Sci. Technol. https://doi.org/10.1016/j.jddst.2019.101174.
Jamróz, E., Kulawik, P., Guzik, P., Duda, I., 2019. The verification of intelligent properties of furcellaran films with plant extracts on the stored fresh Atlantic mackerel during storage at 2 °C. Food Hydrocoll. 97. https://doi.org/10.1016/j.foodhyd.2019.105211.
Jayakumar, A., Radoor, S., Kim, J.T., Rhim, J.W., Parameswaranpillai, J., Nandi, D., Srisuk, R., Siengchin, S., 2022. Titanium dioxide nanoparticles and elderberry extract incorporated starch based polyvinyl alcohol films as active and intelligent food packaging wraps. Food Packag. Shelf Life 34. https://doi.org/10.1016/j.fpsl.2022.100967.
Jonušaite, K., Venskutonis, P.R., Martínez-Hernández, G.B., Taboada-Rodríguez, A., Nieto, G., López-Gómez, A., Marín-Iniesta, F., 2021. Antioxidant and antimicrobial effect of plant essential oils and Sambucus nigra extract in salmon burgers. Foods 10. https://doi.org/10.3390/foods10040776.
Kaur, R., Goyal, D., Agnihotri, S., 2021. Chitosan/PVA silver nanocomposite for butachlor removal: fabrication, characterization, adsorption mechanism and isotherms. Carbohydr. Polym. 262. https://doi.org/10.1016/j.carbpol.2021.117906.
Klinger, M., Jäger, A., 2015. Crystallographic Tool Box (CrysTBox): Automated tools for transmission electron microscopists and crystallographers. J. Appl. Crystallogr. 48, 2012–2018. https://doi.org/10.1107/S1600576715017252.
Krawitz, C., Mraheil, M.A., Stein, M., Imirzalioglu, C., Domann, E., Pleschka, S., Hain, T., 2011. Inhibitory activity of a standardized elderberry liquid extract against clinically-relevant human respiratory bacterial pathogens and influenza A and B viruses. BMC Complement. Altern. Med. 11. https://doi.org/10.1186/1472-6882-11-16.
Kulkarni, N., Muddapur, U., 2014. Biosynthesis of metal nanoparticles: a review. J. Nanotechnol. https://doi.org/10.1155/2014/510246.
Li, K.K., Yin, S.W., Yang, X.Q., Tang, C.H., Wei, Z.H., 2012. Fabrication and characterization of novel antimicrobial films derived from thymol-loaded zein-sodium caseinate (SC) nanoparticles. J. Agric. Food Chem. 60, 11592–11600. https://doi.org/10.1021/jf302752v.
Li, S., Zhang, R., Xie, J., Sameen, D.E., Ahmed, S., Dai, J., Qin, W., Li, S., Liu, Y., 2020. Electrospun antibacterial poly(vinyl alcohol)/Ag nanoparticles membrane grafted with 3,3′,4,4′-benzophenone tetracarboxylic acid for efficient air filtration. Appl. Surf. Sci. 533. https://doi.org/10.1016/j.apsusc.2020.147516.
Lite, M.C., Constantinescu, R., Tănăsescu, E.C., Kuncser, A., Romaniţan, C., Mihaiescu, D. E., Lacatusu, I., Badea, N., 2023. Phytochemical Synthesis of Silver Nanoparticles and Their Antimicrobial Investigation on Cotton and Wool Textiles. Materials 16. https://doi.org/10.3390/ma16113924.
Lu, Y., Fu, K., Zhu, J., Chen, C., Yanilmaz, M., Dirican, M., Ge, Y., Jiang, H., Zhang, X., 2016. Comparing the structures and sodium storage properties of centrifugally spun SnO2 microfiber anodes with/without chemical vapor deposition. J. Mater. Sci. 51, 4549–4558. https://doi.org/10.1007/s10853-016-9768-z.
Manukumar, H.M., Yashwanth, B., Umesha, S., Venkateswara Rao, J., 2020. Biocidal mechanism of green synthesized thyme loaded silver nanoparticles (GTAgNPs) against immune evading tricky methicillin-resistant Staphylococcus aureus 090 (MRSA090) at a homeostatic environment. Arab. J. Chem. 13, 1179–1197. https://doi.org/10.1016/j.arabjc.2017.09.017.
Martínez-Hernández, G.B., Taboada-Rodríguez, A., Marin-Iniesta, F., 2024. Plant bioactive compounds in foods and food packages. Foods 13. https://doi.org/10.3390/foods13091419.
Mejía Suaza, M.L., Leos Rivera, J.C., Rodríguez Padilla, M.C., Moncada Acevedo, M.E., Ossa Orozco, C.P., Zarate Triviño, D.G., 2023. Poly(vinyl alcohol)/Silk Fibroin/Ag-NPs composite nanofibers as a substrate for MG-63 Cells' growth. Polymers 15. https://doi.org/10.3390/polym15081838.
Mirsharifi, S.M., Sami, M., Jazaeri, M., Rezaei, A., 2023. Production, characterization, and antimicrobial activity of almond gum/polyvinyl alcohol/chitosan composite films containing thyme essential oil nanoemulsion for extending the shelf-life of chicken breast fillets. Int. J. Biol. Macromol. 227, 405–415. https://doi.org/10.1016/j.ijbiomac.2022.12.183.
Mohammadi, M., Shahisaraee, S.A., Tavajjohi, A., Pournoori, N., Muhammadnejad, S., Mohammadi, S.R., Poursalehi, R., Hamid Delavari, H., 2019. Green synthesis of silver nanoparticles using Zingiber officinale and Thymus vulgaris extracts: characterisation, cell cytotoxicity, and its antifungal activity against Candida albicans in comparison to fluconazole. IET Nanobiotechnol. 13, 114–119. https://doi.org/10.1049/iet-nbt.2018.5146.
Moldovan, B., David, L., Achim, M., Clichici, S., Filip, G.A., 2016. A green approach to phytomediated synthesis of silver nanoparticles using Sambucus nigra L. fruits extract and their antioxidant activity. J. Mol. Liq. 221, 271–278. https://doi.org/10.1016/j.molliq.2016.06.003.
Mousavian, D., Mohammadi Nafchi, A., Nouri, L., Abedinia, A., 2021. Physicomechanical properties, release kinetics, and antimicrobial activity of activated low-density polyethylene and orientated polypropylene films by Thyme essential oil active component. J. Food Meas. Charact. 15, 883–891. https://doi.org/10.1007/s11694-020-00690-z.
Narath, S., Shankar, S.S., Sivan, S.K., George, B., Thomas, T.D., Sabarinath, S., Jayaprakash, S.K., Wacławek, S., Padil, V.V.T., 2023. Facile green synthesis of Cinnamomum tamala extract capped silver nanoparticles and its biological applications. Ecol. Chem. Eng. S 30, 7–21. https://doi.org/10.2478/eces-2023-0001.
Nasrollahzadeh, M., Sajadi, S.M., Rostami-Vartooni, A., Hussin, S.M., 2016. Green synthesis of CuO nanoparticles using aqueous extract of Thymus vulgaris L. leaves and their catalytic performance for N-arylation of indoles and amines. J. Colloid Interface Sci. 466, 113–119. https://doi.org/10.1016/j.jcis.2015.12.018.
Neves, D., Andrade, P.B., Videira, R.A., de Freitas, V., Cruz, L., 2022. Berry anthocyanin-based films in smart food packaging: a mini-review. Food Hydrocoll. https://doi.org/10.1016/j.foodhyd.2022.107885.
Nguyen, N., Le, C.H., 2021. Synthesis of PVA encapsulated silver nanoparticles as a drug delivery system for Doxorubicin and Curcumin. Int. J. High. Sch. Res. 3, 41–47. https://doi.org/10.36838/v3i3.9.
Nowak, A., Kalemba, D., Krala, L., Piotrowska, M., Czyzowska, A., 2012. The effects of thyme (Thymus vulgaris) and rosemary (Rosmarinus officinalis) essential oils on Brochothrix thermosphacta and on the shelf life of beef packaged in high-oxygen modified atmosphere. Food Microbiol. 32, 212–216. https://doi.org/10.1016/j.fm.2012.05.001.
Ong, K.J., MacCormack, T.J., Clark, R.J., Ede, J.D., Ortega, V.A., Felix, L.C., Dang, M.K. M., Ma, G., Fenniri, H., Veinot, J.G.C., Goss, G.G., 2014. Widespread nanoparticle-assay interference: implications for nanotoxicity testing. PLoS ONE 9. https://doi.org/10.1371/journal.pone.0090650.
Opris, R., Toma, V., Olteanu, D., Baldea, I., Baciu, A.M., Lucaci, F.I., Berghian-Sevastre, A., Tatomir, C., Moldovan, B., Clichici, S., David, L., Florea, A., Filip, G.A., 2019. Effects of silver nanoparticles functionalized with Cornus mas L. extract on architecture and apoptosis in rat testicle. Nanomedicine 14, 275–299. https://doi.org/10.2217/nnm-2018-0193.
Özdemir, D.G., Evcimen Duygulu, N., Özarslan, A.C., Ciftci, F., 2024. Fabrication and characterization of Graphene oxide/Fucoidan/Chitosan reinforced Poly(vinyl alcohol) nanocomposites. J. Mol. Struct. 1301, 137330. https://doi.org/10.1016/J.MOLSTRUC.2023.137330.
Pal, G., Rai, P., Pandey, A., 2018. Green synthesis of nanoparticles: A greener approach for a cleaner future. In: Green Synthesis, Characterization and Applications of Nanoparticles, pp. 1–26. https://doi.org/10.1016/B978-0-08-102579-6.00001-0.
Parveen, K., Banse, V., Ledwani, L., 2016. Green synthesis of nanoparticles: their advantages and disadvantages. AIP Conf. Proc. https://doi.org/10.1063/1.4945168.
Peppas, N.A., Merrill, E.W., 1976. Differential scanning calorimetry of crystallized PVA hydrogels. J. Appl. Polym. Sci. 20, 1457–1465. https://doi.org/10.1002/app.1976.070200604.
Popova, T.P., Ignatov, I., Petrova, T.E., Kaleva, M.D., Huether, F., Karadzhov, S.D., 2022. Antimicrobial activity in vitro of cream from plant extracts and nanosilver, and clinical research in vivo on veterinary clinical cases. Cosmetics 9. https://doi.org/10.3390/cosmetics9060122.
Prabhu, S., Poulose, E.K., 2012. Silver nanoparticles: mechanism of antimicrobial action, synthesis, medical applications, and toxicity effects. Int. Nano Lett. 2. https://doi.org/10.1186/2228-5326-2-32.
Rajeshkumar, S., Bharath, L.V., 2017. Mechanism of plant-mediated synthesis of silver nanoparticles – A review on biomolecules involved, characterisation and antibacterial activity. Chem.-Biol. Interact. https://doi.org/10.1016/j.cbi.2017.06.019.
Roy, A., Bulut, O., Some, S., Mandal, A.K., Yilmaz, M.D., 2019. Green synthesis of silver nanoparticles: Biomolecule-nanoparticle organizations targeting antimicrobial activity. RSC Adv. https://doi.org/10.1039/c8ra08982e.
Saquing, C.D., Manasco, J.L., Khan, S.A., 2009. Electrospun nanoparticle-nanofiber composites via a one-step synthesis. Small 5, 944–951. https://doi.org/10.1002/smll.200801273.
Sau, S., Kundu, S., 2022. Variation in structure and properties of poly(vinyl alcohol) (PVA) film in the presence of silver nanoparticles grown under heat treatment. J. Mol. Struct. 1250. https://doi.org/10.1016/j.molstruc.2021.131699.
Sharma, R., Acharya, A.D., Moghe, S., Shrivastava, S.B., Gangrade, M., Shripathi, T., Ganesan, V., 2014. Effect of cobalt doping on microstructural and optical properties of nickel oxide thin films. Mater. Sci. Semicond. Process. 23, 42–49. https://doi.org/10.1016/j.mssp.2014.02.004.

Sidor, A., Gramza-Michałowska, A., 2015. Advanced research on the antioxidant and health benefit of elderberry (Sambucus nigra) in food - a review. J. Funct. Foods. https://doi.org/10.1016/j.jff.2014.07.012.

Sinha, S., Chatterjee, S.K., Ghosh, J., Meikap, A.K., 2014. Dielectric relaxation and AC conductivity behaviour of polyvinyl alcohol-HgSe quantum dot hybrid films. J. Phys. D Appl. Phys. 47. https://doi.org/10.1088/0022-3727/47/27/275301.

Taghavi, S.M., Larson, R.G., 2014. Regularized thin-fiber model for nanofiber formation by centrifugal spinning. Phys. Rev. E Stat. Nonlinear Soft Matter Phys. 89. https://doi.org/10.1103/PhysRevE.89.023011.

Velásquez, P., Bustos, D., Montenegro, G., Giordano, A., 2021. Ultrasound-assisted extraction of anthocyanins using natural deep eutectic solvents and their incorporation in edible films. Molecules 26. https://doi.org/10.3390/molecules26040984.

Vinicius de Oliveira Brisola Maciel, M., da Rosa Almeida, A., Machado, M.H., Elias, W.C., Gonçalves da Rosa, C., Teixeira, G.L., Noronha, C.M., Bertoldi, F.C., Nunes, M.R., Dutra de Armas, R., Manique Barreto, P.L., 2020. Green synthesis, characteristics and antimicrobial activity of silver nanoparticles mediated by essential oils as reducing agents. Biocatal. Agric. Biotechnol. 28. https://doi.org/10.1016/j.bcab.2020.101746.

Wang, S., Bai, J., Li, C., Zhang, J., 2Wang, S., Bai, J., Li, C., Zhang, J., 2012. Functionalization of electrospun β-cyclodextrin/polyacrylonitrile (PAN) with silver nanoparticles: Broad-spectrum antibacterial property. Appl. Surf. Sci. 261, 499–503. https://doi.org/10.1016/j.apsusc.2012.08.044.

Wang, L., Shi, J., Liu, L., Secret, E., Chen, Y., 2011. Fabrication of polymer fiber scaffolds by centrifugal spinning for cell culture studies. : Microelectron. Eng. 1718–1721. https://doi.org/10.1016/j.mee.2010.12.054.

Wang, M., Wang, Z., Li, S., Wang, Z., Zhao, J., 2015. Mediated electrochemical method for the analysis of membrane damage effects of phenolic compounds to Staphylococcus aureus. J. Electroanal. Chem. 757, 44–50. https://doi.org/10.1016/j.jelechem.2015.09.007.

Wei, X., Yao, J., Wang, F., Wu, D., Zhang, R., 2022. Extraction, isolation, structural characterization, and antioxidant activity of polysaccharides from elderberry fruit. Front. Nutr. 9. https://doi.org/10.3389/fnut.2022.947706.

Yanilmaz, M., Lu, Y., Zhu, J., Zhang, X., 2016. Silica/polyacrylonitrile hybrid nanofiber membrane separators via sol-gel and electrospinning techniques for lithium-ion batteries. J. Power Sources 313, 205–212. https://doi.org/10.1016/j.jpowsour.2016.02.089.

Zhang, Z., Wu, Y., Wang, Z., Zou, X., Zhao, Y., Sun, L., 2016. Fabrication of silver nanoparticles embedded into polyvinyl alcohol (Ag/PVA) composite nanofibrous films through electrospinning for antibacterial and surface-enhanced Raman scattering (SERS) activities. Mater. Sci. Eng. C 69, 462–469. https://doi.org/10.1016/j.msec.2016.07.015.

Zhou, F., He, D., Ren, G., Yarahmadi, H., 2024. In situ and bio-green synthesis of silver nanoparticles immobilized on zeolite as a recyclable catalyst for the degradation of OPDs. Sci. Rep. 14. https://doi.org/10.1038/s41598-024-51271-9.